BASICS OF ULTRASOUND AND PHOTOACOUSTIC IMAGING

Junyu Chen
jchen245@jhmi.edu
Johns Hopkins University

July 22, 2021

Contents

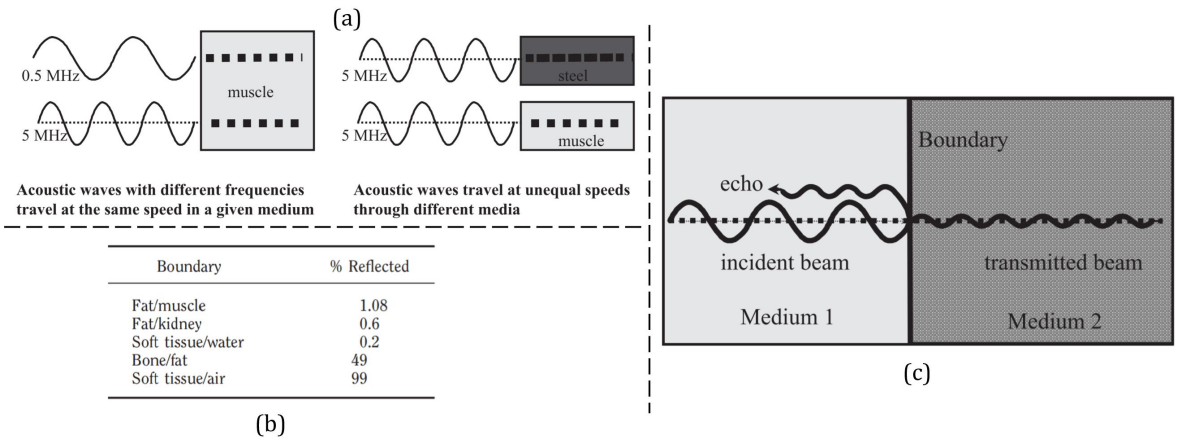

Figure 1: Graphical illustration of the sinusoidal positional embedding. (Images were obtained from [1])

1 Ultrasound Imaging Systems

There are two basic principles regarding how ultrasound is generated and an image is formed. In ultrasound imaging, a transducer generates acoustic waves via the **piezoelectric effect**. When an electric current is applied to the crystals, the crystals deform and vibrate. This deformation produces the ultrasound beam. An ultrasound image is formed via the **pulse-echo principle**. Ultrasound waves are produced in pulses, because the same crystals are used to generate and receive acoustic waves, and they cannot do both at the same time. As the ultrasound pulse enters the patient, it is bounced or reflected back to the transducer. An ultrasound image is formed by measuring the amplitude and the travel time of the reflected sound echoes to reach the transducer. If there is a high acoustic impedance mismatch between two tissue interfaces, then the reflected echo will have a high amplitude resulting in a high-intensity pixel appearance in the formed ultrasound image.

1.1 Physics of Ultrasound Imaging

1.1.1 Frequency

The frequency of an ultrasound wave has a meaning of the number of cycles or pressure changes that occur in 1 second. Ultrasound is sound with a frequency $\geq$ 20 kHz (above the frequency of human audible sound). Typical ultrasound frequency used for clinical purpose are in the range of $[2 \text{ MHZ}, 10 \text{ MHz}]$.

1.1.2 Propagation speed

The speed at which ultrasound can travel through a medium, which is about *1540* meters/second for soft tissue. The speed depends solely on the density and stiffness of the medium. Images in Fig 1 (a) demonstrate the speed and frequency of ultrasound wave.

1.1.3 Ultrasound Interaction with Tissue

When a beam of ultrasound travels through a medium, a reflection of the beam can happen. This reflection is called an *echo*. The production and detection of the echos form the basis of ultrasound imaging. A reflection occurs at the boundary between two materials, provided that the acoustic impedance of the materials is different. Acoustic impedance is calculated as the product of the tissue density and the speed of the sound wave:

$$Z = \rho \times c, \tag{1}$$

where ρ is the density of the tissue, and c is the speed of the sound. If two materials have the same acoustic impedance, their boundary will not produce a reflection (i.e., echo). If the difference in acoustic impedance is large, a strong echo (i.e., large amplitude) will be produced, and vice versa. If the difference in acoustic impedance is too large, all the ultrasounds will be reflected. As shown in Fig. 1 (b), regions containing bone or air can produce large echos that not enough ultrasound remains to image the tissues underneath. Strong reflection or echos show on the ultrasound image as white and weaker echos as gray.

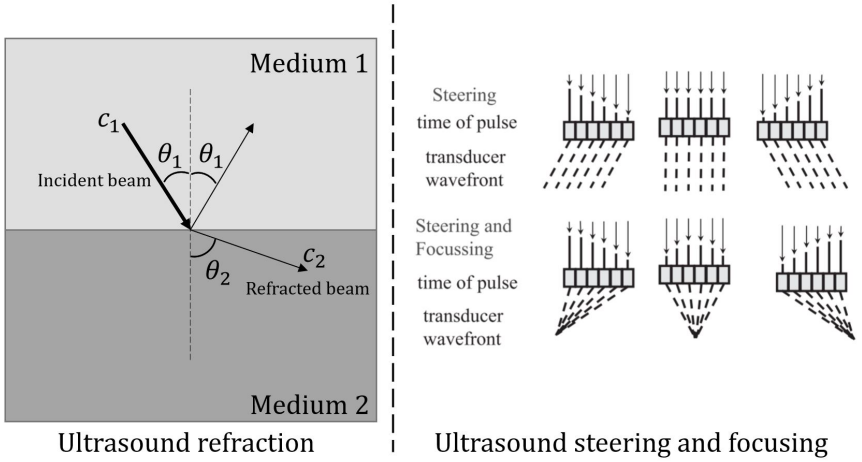

Figure 2: Left: Ultrasound refraction and Snell's law. Right: Ultrasound steering and focusing (image was obtained from [1])

1.1.4 Angle of Incidence

The percentage reflections shown in Fig. 1 (b) are applicable for a normal angle of incidence (90° to the boundary). If a beam of ultrasound strikes a boundary with an angle other than 90°, the echo will return from the boundary at angle equal to the angle of incidence, and the transmitted beam will be deviated from the straight line by an amount that depends on the difference in the velocity of ultrasound. This deviation of the beam traveling direction is known as refraction, and it is governed by the Snell's law (as shown in the left panel Fig. 2):

$$\frac{\sin\theta_1}{c_1} = \frac{\sin\theta_2}{c_2}, \tag{2}$$

where $\sin\theta_1$ and $\sin\theta_2$ are incident and refracted angles of the ultrasound beam, respectively, and c_1 and c_2 denote, respectively, the speed of sound in the first and second medium. Ultrasound machine always assumes that the ultrasound travels in a straight line, therefore, refraction only confuses the machine. However, refraction from rough surfaces produces echoes in many directions, which enables sound to get back to the transducer from oblique surfaces.

1.1.5 Attenuation

The intensity of an ultrasound beam is reduced by attenuation due to reflection, refraction, scattering, and absorption. Reflection and refraction occur at surfaces that are large compared with the wavelength of the ultrasound. For objects that are smaller than the wavelength, the energy of the ultrasound is scattered in many directions and eventually gets absorbed as particle vibration and heat generation. Therefore a high-frequency (smaller wavelength) beam will be attenuated more than a lower frequency (larger wavelength). To penetrate deep into the body, one needs to use a lower-frequency transducer (larger wavelength). However, only higher frequencies can enable finer details. Therefore, there is a trade-off between resolution and depth of penetration for different imaging applications.

In ultrasound, relative intensity of the beam is important. Because the change in intensity is so large, the relative change in intensity is measured in decibels (dB):

$$10\log(\frac{\text{transmitted intensity}}{\text{incident intensity}}). \tag{3}$$

A 3-MHz beam will be attenuated 3dB in the first centimeter (decreased to its 50% intensity), then another 3dB in the next centimeter. Therefore, after passing through 20 centimeters of tissue and being reflected back to the transducer, the intensity will be attenuated by a factor of more than a million.

1.2 Transducers

Transducer is the most critical component in any ultrasonic imaging system. Transducers use a piezoelectric material with a characteristic acoustic impedance perfectly matched to that of the (human) body. Transducers have high efficiency as a transmitter and have high sensitivity as a receiver. However, due to the 99.9% reflection rate of

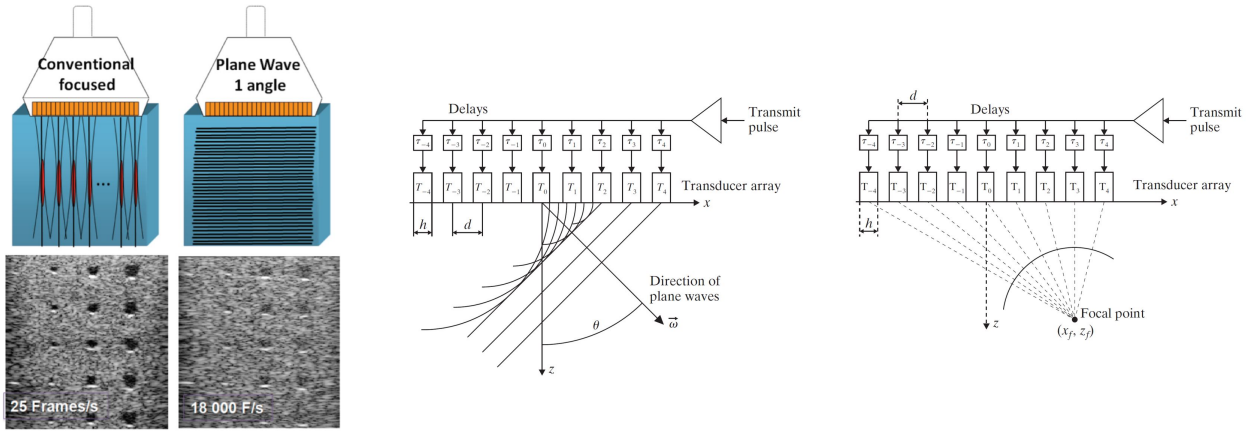

Figure 3: Left: Comparisons between the focused ultrasound beam and the plane wave transmission. Middle: Plane wave steering. Right: Steering and focusing. (images were obtained from [2] and [3])

air/soft-tissue (as shown in Fig. 1 (b)), transducers must be directly coupled to the patient skin without any air gap. This coupling is accomplished by using gel or oil between transducer and human skin.

1.3 Wave Equation

From the physical properties of matter, an acoustic pressure p must satisfy the *wave equation*:

$$\nabla^2 p(x,y,z,t) = \frac{1}{c^2}\frac{\partial^2 p(x,y,z,t)}{\partial t^2} \tag{4}$$

1.4 Ultrasound Beams

Generally, there are two types of ultrasound beams, the plane wave transmission and the focused beam. There differences can be visualized in Fig. 3.

1.4.1 Plane Wave

Ultrasound transducer can generate an acoustic wave that varies in only one spatial direction and time, this is called a *plane wave*. For a plane wave traveling in the z-direction, the wave equation can be reduced to:

$$\frac{\partial^2 p(z,t)}{\partial z^2} = \frac{1}{c^2}\frac{\partial^2 p(z,t)}{\partial t^2}. \tag{5}$$

It is possible to steer the acoustic beam by adding a separate delay element to each transducer a phase array (as shown in the right panel of Fig. 2).

1.4.2 Focused Beam

By tuning the delays in the pulsing of elements, the beam from an array can also be focused, then the beam can sweep as in a scanning motion (as shown in the right panel Fig. 2).

Assuming that transducer T_0 generates a pulse at $t = 0$, then at time t, the leading edge of the pulse generated by T_0 has traveled distance $r_0(t) = ct$. Therefore, the distance between T_i and the wavefront can be expressed as:

$$r_i(t) = r_0(t) - id\sin\theta. \tag{6}$$

Thus, to generate a pulse that will also have the same wavefront, the pulse must be generated at time:

$$t_i = \frac{r_0(t) - r_i(t)}{c} = \frac{id\sin\theta}{c}. \tag{7}$$

To focus the beam, which is a refinement of steering, as shown in the right panel of Fig. 3. The range from T_i to the focal point at (x_f, z_f) is:

$$r_i = \sqrt{(id - x_f)^2 + z_f^2}. \tag{8}$$

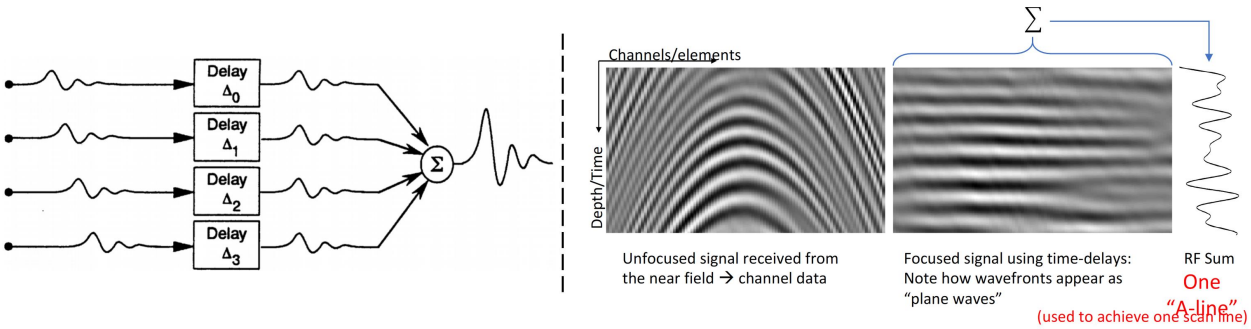

Figure 4: A simple illustration of the delay and sum beamformer.

Therefore, the T_i must fire at:

$$t_i = \frac{r_0 - r_i}{c} = \frac{\sqrt{x_f^2 + z_f^2} - \sqrt{(id - x_f)^2 + z_f^2}}{c}. \tag{9}$$

2 Photoacoustic Imaging

In photoacoustic (PA) imaging, ultrasound waves are produced by irradiating the tissue with modulated electromagnetic radiation, usually pulsed on a nanosecond timescale. In the case of optical excitation, absorption by specific tissues such as hemoglobin, melanin, or water followed by rapid conversion to heat produces a small temperature rise. This rise of temperature (i.e., thermal expansion) leads to an initial pressure increase, which then subsequently relaxes, resulting in the emission of broadband low-amplitude acoustic waves. The acoustic waves propagate through the tissue to the surface, where they are detected by the ultrasound receiver. By measuring the time of arrival of the acoustic waves and knowing the speed of sound in tissue, a PA image can be reconstructed in the same way that a pulse-echo ultrasound image is formed. The acoustic pressures in PA are several orders of magnitude smaller than that in ultrasound.

2.1 Source of Contrast

In ultrasound, an image represents the acoustic impedance mismatch between different tissues. A PA image, however, is absorption-based. It represents the initial pressure distribution produced by the deposition of the optical energy, which depends on the optical absorption and scattering properties of the tissue [4]. PA imaging can provide greater tissue differentiation and specificity than ultrasound because difference in optical absorption of tissues can be much larger than the difference in acoustic impedance. PA imaging thus provides the ability to distinguish any structure that has a higher optical absorption than surrounding tissue, some examples are blood vessels and nerves.

Although PA imaging can provide larger tissue differentiation, it comes at a cost, the penetration depth, which is limited due to the strong optical attenuation exhibited by most tissue. To understand the contrast produced by PA imaging, we need to understand how the PA signal is created:

- A pulsed laser light is incident on the tissue surface. Depending on the wavelength, the light penetrates to some depth.
- The light is then scattered and absorbed by the tissue.
- The absorbed laser energy is converted into heat in the tissue, which produces an initial pressure increase of the tissue, and later emits the acoustic waves.
- The acoustic waves propagate back to the surface and are detected by the transducer.

The dominance of optical absorption as the primary source of PA image contrast lends PA imaging to the visualization of anatomical features that contain an abundance of chromophores (i.e., light-absorbing molecules) such as hemoglobin, lipids, and water.

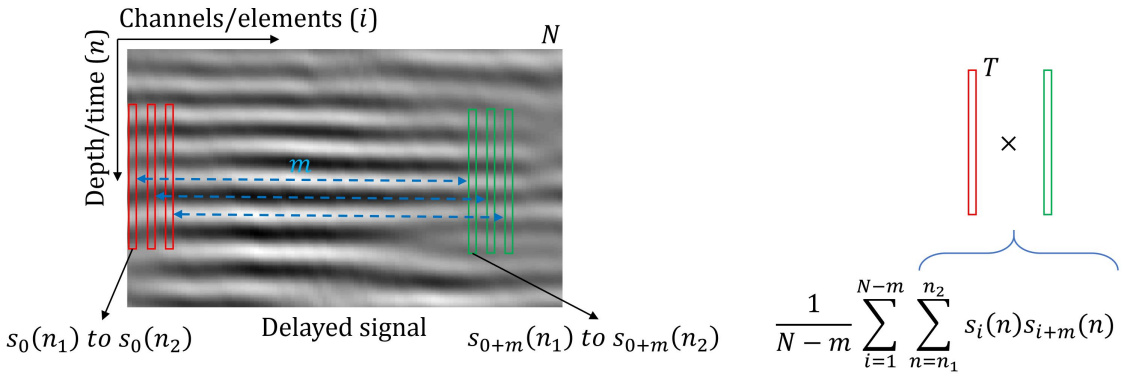

Figure 5: An illustration of the short lag spatial coherence beamforming.

2.2 Basic Imaging Equation

With a pulsed laser, the local fractional volume expansion can be expressed as [5]:

$$\frac{dV}{V} = -\kappa p(\overrightarrow{r}) + \beta T(\overrightarrow{r}), \tag{10}$$

where κ is the isothermal compressibility, β is the thermal coefficient of volume expansion, and $p(\overrightarrow{r})$ and $T(\overrightarrow{r})$ are, respectively, changes in pressure and temperature. A typical laser pulse duration is smaller than the thermal confinement and the stress confinement time. In this case, the fractional volume expansion $\frac{dV}{V}$ is negligible. Therefore, the initial photoacoustic pressure $p(\overrightarrow{r})$ can be expressed as:

$$p(\overrightarrow{r}) = \frac{\beta T(\overrightarrow{r})}{\kappa}, \tag{11}$$

where the temperature rise can be expressed as a function of optical absorption:

$$T = \frac{\Gamma F(r)}{\rho C_v}. \tag{12}$$

Then, the initial photoacoustic pressure can be written as:

$$p_0(r) = \frac{\beta \mu_a(r) F(r)}{\rho C_v \kappa} = \Gamma \mu_a(r) F(r). \tag{13}$$

Here Γ is the Grueneisen parameter, which increases as the temperature rises, $\mu_a(r)$ is the absorption coefficient, and $F(r)$ denotes the local optical fluence (i.e., the optical energy delivered per unit area). PA images are often described as being 'absorption based', because the initial acoustic pressure depends on the absorption coefficient. However, it is worthing noting that this does not mean that image contrast is directly proportional to the absorption coefficient μ_a. It is in fact proportional to the product of μ_a and F_a, so p_0 is a nonlinear function of μ_a.

3 Beamforming in Ultrasound and PA

3.1 Delay and Sum

Delay and Sum (DAS) is the most standard technique in ultrasound and PA beamforming (as shown in Fig. 4). DAS is mathematically defined as [6]:

$$y_{DAS}(k) = \sum_{i}^{M} x_i(k - \Delta_i), \tag{14}$$

where $y_{DAS}(k)$ denotes the output of the beamformer of the k^{th} time index (or depth), M denotes the number of the array elements, and $x_i(k)$ and Δ_i are the detected signals and the corresponding time delay for detector i.

3.2 Short-lag Spatial Coherence

Instead of the simple summation, the time delayed signal can be used in a more advanced beamformer, namely the short-lag spatial coherence (SLSC). SLSC beamforming only accounts for the similarity across the received signals in the aperture domain, as a function of element separation m. Then, an SLSC image is formed as the integral of the spatial coherence function over the first M lags. It displays spatial coherence between the received echos at different short-lag values (i.e., element separation m), thereby reduces speckle noise and removes clutter artifacts. As shown in Fig. 5, for a receive aperture with N elements, the *time-delayed* signal detected by the i^{th} element of n^{th} time index (or depth) is defined as $s_i(n)$ (note that $s_i(n)$ is a zero-mean signal). The estimated spatial covariance across the receive aperture is defined as [7]:

$$\hat{C}(m) = \frac{1}{N-m} \sum_{i=1}^{N-m} \sum_{n=n_1}^{n_2} s_i(n) s_{i+m}(n), \tag{15}$$

where m is the distance, or lag, which is really the number of elements between two points in the aperture. Notice that signals s_i and s_{i+m} have zero-mean. The covariance, $\hat{C}(m)$, is further normalized by the individual variances of the signals s_i and s_{i+m}, the spatial correlation can be computed by:

$$\hat{R}(m) = \frac{1}{N-m} \sum_{i=1}^{N-m} \frac{\sum_{n=n_1}^{n_2} s_i(n) s_{i+m}(n)}{\sum_{n=n_1}^{n_2} s_i(n) \sum_{n=n_1}^{n_2} s_{i+m}(n)}. \tag{16}$$

It is found that the largest losses in spatial coherence will occur in the regions of low lags [7]. Therefore, the short-lag spatial coherence (SLSC) is computed as the integral of the spatial coherence function over the first M lags:

$$R_{sl} = \int_1^M \hat{R}(m) dm = \sum_{m=1}^{M} \hat{R}(m), \tag{17}$$

where M is a hyperparameter, for which a parameter Q is introduced to represent Q as a percentage of the aperture width N:

$$Q = \frac{M}{N} \times 100\% \tag{18}$$

3.3 Locally Weighted Short-lag Spatial Coherence

Instead of summing up to a pre-defined lag value of M, LW-SLSC computes the weighted sum of a subset of the coherence functions $\hat{R}_i(m)$. $\hat{R}_i(m) \in \mathbb{R}^{k_z \times k_x \times N}$ is the i^{th} moving kernel inside the correlation matrix $\hat{R}(m) \in \mathbb{R}^{N_z \times N_x \times N}$. The weighting parameter $w_i(m)$ for each coherence function in side the moving kernel (i.e., $\hat{R}_i(m)$) is determined by optimizing an energy function [8]:

$$\hat{w_i} = \arg\min_{w_i} \text{TV}(f(w_i, \hat{R}_i)) + \alpha^2 \|\nabla w_i\|^2, \tag{19}$$

where

$$f(w_i, \hat{R}_i) = \sum_{m=1}^{N} \hat{R}_i(m) \cdot w_i(m), \tag{20}$$

$$\|w_i\| = 1, \text{ and } 0 \leq w_i \leq 1. \tag{21}$$

The key advantage of LW-SLSC is the adaptive selection of the number of lags to be summed, which reduces incoherent signals and noise. The kernel size ($k_z \times k_x$), overlap, and the regularization term are all factors that influence the quality of LW-SLSC.

4 Noise and artifacts in ultrasound and PA

4.1 Speckle Noise

Speckle noise comes from the acoustic echoes with random phases and amplitudes. The superposition of these echos produces a complicated interference pattern, which is known as speckle noise. Speckle noise is a pseudo-random process because it generally depends on the structure of the tissue. Speckle noise tends to reduce the image contrast and blur the image details.

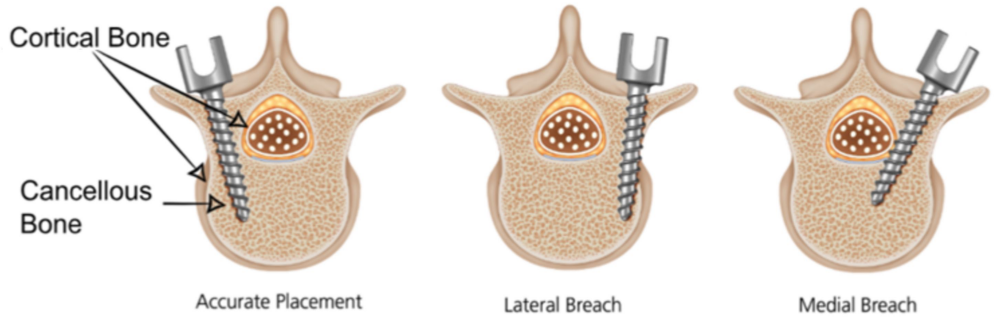

Figure 6: Examples of accurate and inaccurate pedicle screw placement. (Image obtained from [9])

4.2 Reverberation

Reverberation artifacts appear as a sequence of lines that are evenly spaced. An ultrasonic beam bounces back and forth between two highly reflecting contacts or between the transducer and a strong reflector to produce the artifacts. An illustrative diagram of this artifact is shown here https://radiopaedia.org/cases/reverberation-artifact?lang=us.

4.3 Mirror Image

One of the beam path artifacts is the mirror image artifact. When an ultrasound beam hits a reflecting surface, it is not reflected directly back to the transducer, but instead takes an indirect return back. An illustrative diagram of this artifact is shown here https://litfl.com/mirror-image-artefacts/.

4.4 Acoustic shadowing

The sound beam is completely absorbed or reflected at the structure with high attenuation, resulting in a shadow underneath the high acoustic attenuating object. An illustrative diagram of this artifact is shown here https://okean.rs/artifacts-in-ultrasonography/.

4.5 Acoustic enhancement

Acoustic enhancement is a localized increase in echo amplitude distal to a low-attenuation structure that appears as a brighter region. There is less tissue reflection when sound waves pass through a poorly attenuating structure that allows them easy passage, and an area of artifactually increased echogenicity is produced right under the structure because more sound waves are present in this area compared to tissues at the same depth around it. An illustrative diagram of this artifact is shown here https://okean.rs/artifacts-in-ultrasonography/.

4.6 Clutter

Clutter in ultrasound and PA originates from the scattering by multiple tissues (i.e., multipath scattering). Clutter typically overlays structures or signals of interest and often degrades image contrast.

5 Image Quality for Ultrasound and PA

The following paragraphs introduce the commonly used image quality measurements in ultrasound and PA. Varaibles include the mean of regions within and outside a target of interest, denoted by μ_i and μ_o, respectively, the standard deviation of the same regions (σ_i and σ_o), and the histograms of the same regions (h_i and h_o).

Contrast Contrast measures visibility of the target with respect to the background. It is defined as:

$$\text{Contrast} = 20\log_{10}(\frac{\mu_i}{\mu_o}). \tag{22}$$

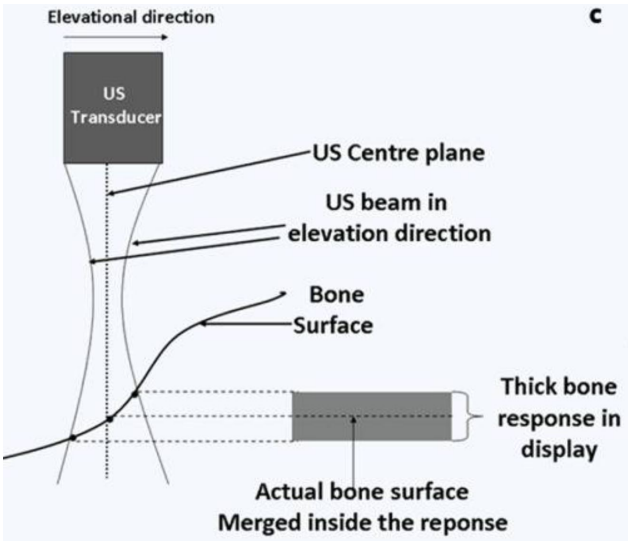

Figure 7: Bone boundary has thickness due to the inclination. (Image obtained from [10])

Signal-to-noise ratio SNR relates signal to inherent imaging system noise. It is defined as:

$$SNR = \frac{\mu_i}{\sigma_0}. \tag{23}$$

Contrast-to-noise ratio CNR measures the detectability of a specific target. It is defined as:

$$CNR = \frac{|\mu_i - \mu_o|}{\sqrt{\sigma_i^2 + \sigma_o^2}}. \tag{24}$$

Generalized contrast-to-noise ratio CNR is sensitive to dynamic range alterations. gCNR overcomes this shortcoming by consider the intensity histograms within and outside the target region. It is defined as:

$$gCNR = 1 - \sum_{k=0}^{N-1} \min h_i(x_k), h_o(x_k). \tag{25}$$

-6 dB FWHM of photoacoustic signals It enables measurements of resolution, which is necessary for comparison to the allowable tolerance and accuracy of a specified surgical or interventional task.

6 Application of Ultrasound and PA in Bone

One of the applications of ultrasound and PA bone imaging is to assist spinal fusion surgeries in real-time. Spinal fusion is surgery to connect two or more vertebrae in the spine permanently. It is done by placing screws through the pedicles of vertebrae to connect them with a metal rod and stabilize the spine. It is critical to ensure the correct trajectory during the hole creation process in order to avoid accidental bone breaches and screw misplacement, as shown in Fig. 6.

6.1 Ultrasound of bone

Ultrasound images are formed by measuring the amplitude and the travel time of the reflected sound echoes to reach the US transducer. If there is a high acoustic impedance mismatch between two tissue interfaces the reflected sound echo signal will have a high amplitude resulting in a high-intensity pixel appearance in the formed US image. A high-intensity pixel in an US image indicates a strong likelihood of the presence of a boundary, such as soft tissue interface or bone. Since bone tissue has one of the highest acoustic impedance values compared to other tissues such as muscle, fat, liver, or water, most of the signal is reflected back from the bone interface resulting in a high-intensity feature in the reconstructed US image. This high-intensity bone feature is followed by a region with very low-intensity values appearing right after bone boundary. This low-intensity region, “shadow region”, is one of the typical US

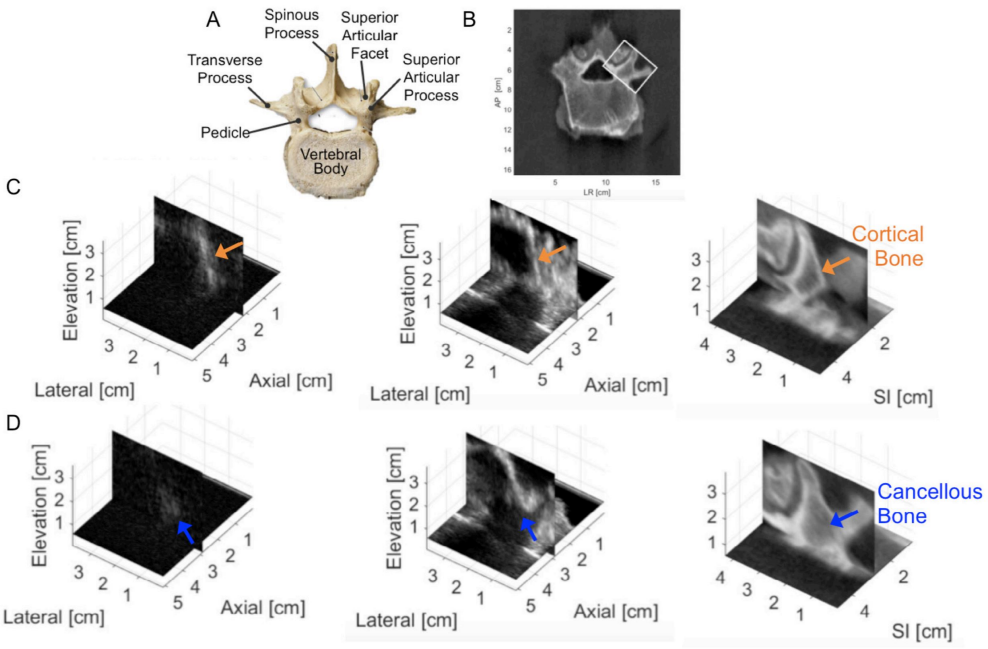

Figure 8: Bone boundary has thickness due to the inclination. (Image obtained from [11])

imaging artifacts denoting that interior bone surfaces cannot be imaged with US imaging. The high-intensity feature depicting bone boundary response looks like a line with a shape closely resembling the surface. However, compared to bone surface appearance in CT or fluoroscopy imaging, the surface response in US is not a sharp transition region but rather has a thickness that can reach a value of 4 mm in certain cases. The response thickness is affected by the inclination of the image surface with respect to the US transducer. The greater the inclination of the imaged surface, the greater the response thickness (as shown in Fig. 7).

6.2 PA of bone

Photoacoustic imaging has been explored as an option to uncover expected differences between the cortical and cancellous bone for the potential guidance of spinal fusion surgery. An optical fiber that delivers laser light could either be isolated from or attached to the surgical tool. A standard clinical ultrasound probe would then be placed with acoustic coupling gel on the vertebra of interest. This ultrasound probe aims to receive the acoustic response generated by optical absorption within the blood-rich cancellous core. Although it is hard for an ultrasound to travel through cortical bone, it is possible for the acoustic pressure response of the cancellous core (resulting from the absorption of the laser pulse) to travel through the 244 μm to 1.75 mm-thick cortical bone layer covering the cancellous core. Therefore, in this application of photoacoustic imaging for surgical guidance, blood-rich regions can be targeted rather than avoided. The difference between the PA images obtained by pointing optical fiber toward the cortical bone and the cancellous core of the pedicle can be observed from Fig. 8. The PA image of the cancellous bone has lower amplitudes and is more diffuse. This difference is achievable because the optical absorption of blood is orders of magnitude higher than that of bone, which permits a photoacoustic response from the blood-rich cancellous core.

6.2.1 Pre-insertion of screw

The trajectory of fiber position affects the appearance of the resulting PA image (as shown in Fig. 9). Generally, a good fiber position yields deeper signals corresponding to the response from the blood-rich cancellous core. This information can be used to target an optimal position before inserting the screw.

6.2.2 During the screw insertion

When placing the screw inside the vertebra during spinal fusion surgery, it is important to prevent breaching the pedicle wall (which consists of cortical bones). Thus, it is desirable to be able to differentiate cortical bones from cancellous bones in real-time during the operation. Real-time PA imaging can be used to identify cortical bone from cancellous bone. The laser light pulses can be delivered through the tip of the drill while it is being inserted into the

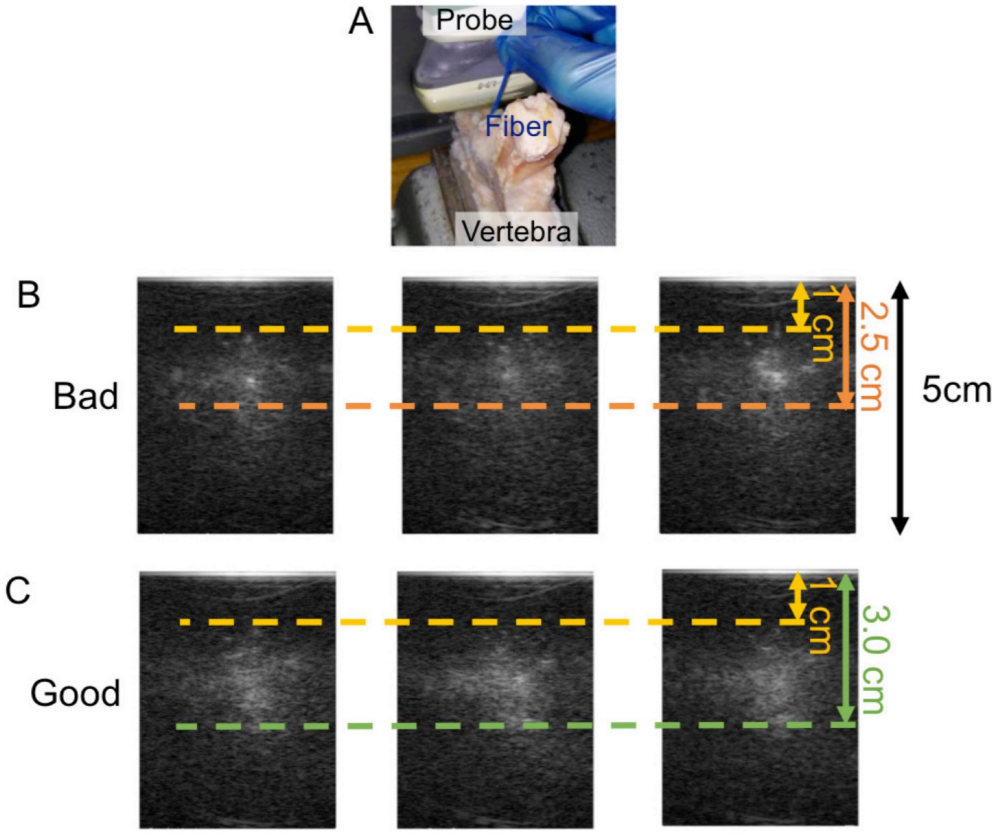

Figure 9: Fiber position affects the appearances of the PA images. (Image obtained from [11])

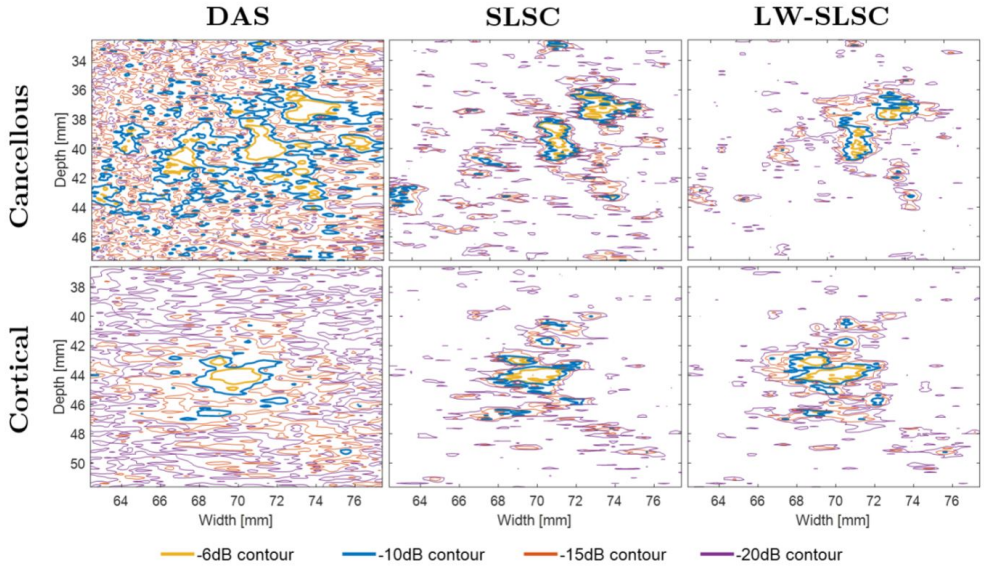

Figure 10: Contour plots of photoacoustic DAS, SLSC, and LW-SLSC images. (Image obtained from [9])

pedicle to create a hole for the screw. The differences in the PA image appearance of cortical and cancellous bones can be identified. Three beamforming techniques can be used to reconstruct PA images, delay-and-sum (DAS), short-lag spatial coherence (SLSC), and locally weighted short-lag spatial coherence (LW-SLSC). These beamforming methods are described in section 3. As shown in Fig. 10, PA differentiation of cortical and cancellous bones is possible with DAS beamformer at a contour level of -6 dB. The -6 dB contour is optimal because it allows more localized visualization of the PA response from the fiber tip without confusing this response from that of surrounding tissue. The blood-rich cancellous bone generates incoherent signals, speckle noise, and clutter. These artifacts are possible to be observed in DAS image. On the other hand, coherence-based PA imaging removes the dependence on optical absorption. Unlike a DAS image, where the intensity is dependent on the received pressure amplitude (which then depends on the optical absorption for PA imaging). A coherence-based image only accounts for and displays the similarities of the received waves. Therefore, the dependence on optical absorption is completely ignored. However, PA imaging enables the localization of fiber tips for tip tracking applications. The improved localization of the tooltip can be appreciated by estimating the centroid of the -6 dB contour levels for the SLSC and LW-SLSC images.

The DAS PA image would show a diffuse pattern when the drill is inside the pedicle and touching the cancellous core. This diffuse pattern is caused due to the acoustic waves reflect within the blood-rich structure of the cancellous bone, which affects the alignment of the delayed signals during the beamforming process. On the other hand, when the drill breaches the cortical wall, a well-defined, compact signal can be observed. This is because the cortical walls are denser than cancellous bone, which is expected to produce fewer signal reflections. However, this differentiation cannot be seen when a coherence-based beamformer is used. These beamformers would reduce the incoherent signals associated with the cancellous bone, which is a necessary feature for differentiating bone types. Nevertheless, a coherence-based beamformer enables the localization of the coherent signal source (i.e., the tip of the drill).

References

[1] John E Aldrich. Basic physics of ultrasound imaging. *Critical care medicine*, 35(5):S131–S137, 2007.

[2] Mickael Tanter and Mathias Fink. Ultrafast imaging in biomedical ultrasound. *IEEE transactions on ultrasonics, ferroelectrics, and frequency control*, 61(1):102–119, 2014.

[3] Jerry L Prince and Jonathan M Links. *Medical imaging signals and systems*. Pearson Prentice Hall Upper Saddle River, 2006.

[4] Paul Beard. Biomedical photoacoustic imaging. *Interface focus*, 1(4):602–631, 2011.

[5] Jun Xia, Junjie Yao, and Lihong V Wang. Photoacoustic tomography: principles and advances. *Electromagnetic waves (Cambridge, Mass.)*, 147:1, 2014.

[6] Moein Mozaffarzadeh, Masume Sadeghi, Ali Mahloojifar, and Mahdi Orooji. Double-stage delay multiply and sum beamforming algorithm applied to ultrasound medical imaging. *Ultrasound in medicine & biology*, 44(3):677–686, 2018.

[7] Muyinatu A Lediju, Gregg E Trahey, Brett C Byram, and Jeremy J Dahl. Short-lag spatial coherence of backscattered echoes: Imaging characteristics. *IEEE transactions on ultrasonics, ferroelectrics, and frequency control*, 58(7):1377–1388, 2011.

[8] Eduardo A Gonzalez, Amit Jain, and Muyinatu A Lediju Bell. Combined ultrasound and photoacoustic image guidance of spinal pedicle cannulation demonstrated with intact ex vivo specimens. *IEEE Transactions on Biomedical Engineering*, 2020.

[9] Eduardo Gonzalez, Amit Jain, and Muyinatu A Lediju Bell. Photoacoustic differentiation of cortical from cancellous bone in the lumbar vertebrae of an intact human cadaver to prevent bone breaches during spinal fusion surgeries. In *Photons Plus Ultrasound: Imaging and Sensing 2021*, volume 11642, page 1164210. International Society for Optics and Photonics, 2021.

[10] Ilker Hacihaliloglu. Ultrasound imaging and segmentation of bone surfaces: A review. *Technology*, 5(02):74–80, 2017.

[11] Joshua Shubert and Muyinatu A Lediju Bell. Photoacoustic imaging of a human vertebra: implications for guiding spinal fusion surgeries. *Physics in Medicine & Biology*, 63(14):144001, 2018.